International Journal of Aerospace and Lightweight Structures
Vol. 2, No. 1 (2012) 1–15

DOI:

Topology Optimization of a Bi-Material Plate with Respect to Sound Radiation in a Thermal Environment*

Xiongwei Yang, Gang Chen and Yueming Li[a]
State Key Laboratory for Strength and Vibration of Mechanical Structures,
Xi'an Jiaotong University, Xi'an, 710049, China.
[a] *liyueming@mail.xjtu.edu.cn*

Received date/Month/Year
Revised date/Month/Year

This paper carries out the structural topology optimization to minimize the radiated acoustic power in a thermal environment for the first time. The stress induced by the thermal environment which can reduce the stiffness of the structure, thus changing its radiation property and optimal design. An approach to investigate this effect is presented through studying a baffled bi-material plate. The plate is excited by a harmonic load and subjected to a uniform temperature rise. The thermal stress is first evaluated and considered as pre-stress in the structural dynamic analysis. With the dynamic response, the acoustic power can be obtained using Rayleigh integral. Sensitivity analysis with respect to the design variables is calculated according to the material interpolation model. Some typical cases are studied; the thermal environment is below the critical buckling temperature and the driving frequency is lower than the plate's second natural frequency. Numerical results show that the natural frequencies decrease with the increase of the temperature and the structure tends to resonance; thus the radiated sound power level becomes higher and the pattern of the optimal topology resembles that of the associated mode shape more closely. The sound power level of the optimal plate becomes lower than that of the initial plate, especially for the higher temperature cases. During the optimization process, the critical buckling temperature increases and the structure is always in pre-buckling.

Keywords: Topology optimization, Acoustic power, Thermal environment.

1. Introduction

One of the problems encountered by hypersonic aircrafts is the high thermal and acoustic environments to which the aircraft is subjected during a significant portion of the flight envelope. Severe thermal environment due to aerodynamic heating induces compressive stresses which could cause thermal buckling and alter the natural frequencies. High-intensity acoustic load could cause failure of the structure and dysfunction of the payload. Thus, the structural design for spacecrafts operating

*National Natural Science Foundation of China (91016008,11021202,10902082)

in such extreme environments is of significant importance to provide light-weight structures with good thermal-acoustic properties.

Structural-acoustic design was first carried out in automobile manufactures; Ma and Hagiwara [1991] carried out a coupled structural-acoustic sensitivity analysis of a NVH problem. Belegundu et al [1994] and Salagame et al [1994] described a general way to minimize the sound radiation of a baffled plate. The structure response is first evaluated by numerical method; the acoustic power can be obtained with Rayleigh integral. Christensen and Sorokin et al [1998] reviewed developments in the structural-acoustic analysis and optimization, and typical objective functions and optimization formulations were discussed. Lee and Wang [2003] designed thin structures with respect to radiation and scattering of sound using multi-domain BEM based on the commercial code SYSNOISE. Kim and Dong et al [2003, 2006] employed sequential FEM and BEM to carry out design sensitivity analysis for structural–acoustic problems. The structural dynamic behavior was first obtained through frequency-response analysis, and BEM was used to solve for the pressure response of the acoustic domain.

Since the landmark work of Bendsøe and Kikuchi [1988], topology optimization has been extended to various fields to find the optimal configurations of structures with respect to different criteria. The first application in acoustic design was carried out by Luo and Gea [2003], employing an approach based on topology optimization to study the optimal configuration of stiffeners for the interior sound reduction in a coupled structural-acoustic system. Lee and Wang et al [2004] used the topology optimization to design holes on the thin-body through a normal derivative integral equation. Yoon and Jensen [2007] et al carried out a structural-acoustic optimization using a mixed finite element formulation, in which displacements as well as pressure are the primal variables. Du and Olhoff [2007, 2010] dealt with the topology optimization problems to minimize the sound power or sum of the pressure square radiated from the structural surface(s) into a surrounding acoustic medium. The structural dynamic displacement response was first calculated and then the acoustic pressure was obtained. Akl and El-Sabbagh [2009] developed a mathematical model based on FEM to optimize a plate coupled with an acoustic cavity to reduce the fluid-structure interactions at different structural frequencies, verified through experiment by monitoring the vibration and sound radiation into a rigid acoustic cavity of the optimized plates.

However to the authors' knowledge, there are few works on structural-acoustic topology optimization in thermal environments. It is well known that thermal stress may change the stiffness of structure, thus altering its dynamic characteristic [Zienkiewicz and Taylor, 2005]. Pedersen [2001, 2002] optimized the static compliance or eigenvalues of pre-stressed isotropic and laminated plates. The initial stress was given at different constant levels to study its influence on the topology. In fact, the thermal load induced by the elevated thermal environment is design-dependent load, varying with the design variables [Rozvany, 2001; Bruyneel and Duysinx, 2005;

Gao and Zhang, 2010]. Another particular characteristic of the thermal load is that it involves both the elastic modulus and the thermal expansion coefficient. For topology optimization of bi-material structures as in this work, the penalties of these two parameters should match each other; otherwise incompatibility may occur between stiffness and thermal load. The thermal stress coefficient, i.e. the product of elastic modulus and thermal expansion coefficient has been proposed to characterize the design-dependent property of thermal-load [Rodrigues, 1995; Gao and Zhang, 2010].

In this paper, topology optimization respect to the sound radiation in thermal environments is carried out for the first time. The thermal stress is first evaluated and used to form the geometric stiffness matrix. Then the structural response in the thermal environment is obtained through the stress stiffening dynamic formula. With the dynamic response, the acoustic power can be acquired by Rayleigh integral. Based on the material interpolation model, sensitivity analysis with respect to the design variables is calculated. A bi-material plate subjected to a harmonic force with prescribed amplitude and frequency in a uniform thermal environment is studied. The critical buckling temperature is evaluated to determine the upper limit of the temperature rise, so that a pre-buckling small-deformation can be assumed to establish the dynamic formula in a stress stiffening form [Cook, 1994]. The RAMP interpolation model [Stolpe and Svanberg, 2001] and GCMMA algorithm [Svanberg, 1995] are used in this paper.

2. Dynamic Structure in Thermal Environment

2.1. *Buckling analysis*

When a plate is subjected to temperature rise from the ambient, thermal stress develops in the plate. The thermal stress may induce buckling of the structure when it is high enough. The optimization is carried out when the plate is in pre-buckling state; thus, the critical buckling temperature T_{cr} is first evaluated to determine the upper limit of the uniform temperature rise. An eigenvalue buckling analysis can be stated as [Cook, 1994]

$$(K + \lambda K_G)\,\Phi = 0 \tag{1}$$

where λ is a scalar multiplier, Φ is the eigenvector and K is the stiffness matrix. $\Delta T = T_1 - T_0$is the temperature change.

$$T_{cr} = T_0 + \lambda \Delta T \tag{2}$$

$\mathrm{K_G}$ refers to the geometric stiffness for bending induced by the in-plane thermal stress [Zienkiewicz and Taylor, 2005]

$$\mathrm{K_G} = \sum_e \int_{A_e} G^{\mathrm{T}} S G dA \tag{3}$$

where **S** is the membrane stress matrix at the element level; **G** is the strain-displacement matrix; A_e is the area of the element.

2.2. *Membrane stress*

If the temperature change across the thickness is uniform, the thermo-elastic problem of the plate can be described with the plane-stress constitutive equation,

$$\sigma = D_{\mathrm{m}}\left(\varepsilon - \alpha T\right) = ED\varepsilon - \beta \mathrm{DT} \tag{4}$$

where σ is the membrane stress vector, comprised of the same components as the membrane stress matrix $\mathbf{S}$; E, α, $\beta = E\alpha$ are the elastic modulus, the thermal expansion coefficient and the thermal stress coefficient respectively; $\mathbf{D}_m$ is the membrane elasticity matrix; $\mathbf{T}$ is the temperature rise vector.

The strain in Eq. (4) can be written in FE form

$$\varepsilon = \mathbf{B}\mathbf{u}_{\mathrm{t}i} \tag{5}$$

where $\mathbf{B}$ is the strain-displacement matrix; $\mathbf{u}_{ti}$ is the element displacement vector which can be obtained with the boundary conditions through

$$\mathbf{K}\mathbf{U}_{\mathrm{t}} = \mathbf{F}_{\mathrm{t}} \tag{6}$$

where $\mathbf{F}_t$ is the equivalent thermal force induced by the uniform temperature rise; $\mathbf{U}_t$ is the thermal displacement; the index "t" denotes the word "thermal".

The equivalent membrane thermal force $\mathbf{F}_t$ has the form [Zienkiewicz and Taylor, 2005]

$$\mathrm{F_t} = -\sum_i \int_{A_i} \alpha \mathrm{B}^{\mathrm{T}} \mathrm{D_m T} dA = -\sum_i \int_{A_i} \beta B^{\mathrm{T}} \mathrm{DT} dA \tag{7}$$

Eq. (7) indicates that the equivalent thermal force is design-dependent. For the bi-material topology optimization problem, both the elastic modulus and the thermal expansion coefficient have to be switched simultaneously from one material to the other. Incompatibility may occur between the stiffness and the thermal load. By introducing the thermal stress coefficient β, the penalty can be made properly to the thermal load $\mathbf{F}_t$, and the incompatibility can be efficiently avoided [Gao and Zhang, 2010].

2.3. *Dynamic formula*

When the temperature is below T_{cr}, the dynamic FE formula of the plate in a uniform thermal environment can be written in a stress stiffening form (with the damping neglected) [Cook, 1994]

$$(\mathbf{K} + \mathbf{K}_{\mathrm{G}} - \omega^2 \mathbf{M})\mathbf{U} = \mathbf{F} \tag{8}$$

where $\mathbf{K}$, $\mathbf{M}$ are the stiffness and mass matrices respectively; $\mathbf{F}$ is the amplitude vector of the time-harmonic external load; $\omega = 2\pi f$ is the circle frequency; $\mathbf{U}$ is the dynamic displacement response vector.

Using mode superposition, $\mathbf{U}$ can be represented as

$$\mathbf{U} = \sum_{l}^{m} \lambda_l \Phi_l \tag{9}$$

where λ_l is mode participation factor, m is the number of modes used and Φ_l is the lth eigenvector.

Premultiply Eq. (8) by Φ^{T}

$$\Phi^T(\mathbf{K} + \mathbf{K}_{\mathrm{G}} - \omega 2^{\mathrm{M}})\Phi\lambda = \lambda^{\mathrm{T}}\mathrm{F} \tag{10}$$

Note that $\Phi^{\mathrm{T}}(\mathbf{K} + \mathbf{K}_{\mathrm{G}})\Phi = \mathrm{diag}(\omega_{nl})$ and $\Phi^{\mathrm{T}}\mathrm{M}\Phi = I$, where ω_{nl} is the structural lth natural frequency in the thermal environment.

$$\lambda_l = \sum_{l}^{m} \frac{\Phi - l^{\mathrm{T}}\mathrm{F}}{\omega_{\mathrm{n}l}^2 - \omega^2} \tag{11}$$

3. Finite Element Discretization for Radiated Power

Consider a vibrating plate mounted on a rigid baffle and placed in a light fluid such as air. The pressure p at any observation point $\mathbf{r}$ on the surface of the plate can be described using Rayleigh integral as

$$p = j\rho_0\omega \int_A v_a G(\mathbf{r} - \mathbf{r}_a) dA \tag{12}$$

where v_a refers to the normal surface velocity at point $\mathbf{r}_a$; ρ_0 indicates the density of air; $G(\mathbf{r}\text{-}\mathbf{r}_a)$ is the half-space Green's function

$$G(\mathbf{r} - \mathbf{r}_a) = \frac{e^{-jk|\mathbf{r}-\mathbf{r}_a|}}{2\pi|\mathbf{r} - \mathbf{r}_a|} \tag{13}$$

$k = \omega/c$ is the wave number and c is the speed of sound in air.

The acoustic power radiated from the vibrating plate can then be written as

$$\begin{aligned} W &= \int_A \frac{1}{2} R_e(pv^*) dA \\ &= \frac{j\rho_0\omega}{4\pi} \int_A \int_A v_a \frac{e^{-jk|\mathbf{r}-\mathbf{r}_a|}}{|\mathbf{r} - \mathbf{r}_a|} dA v^* dA \\ &= \frac{\rho_0\omega}{4\pi} \int_A \int_A v_a \frac{\sin k|\mathbf{r} - \mathbf{r}_a|}{|\mathbf{r} - \mathbf{r}_a|} dA v^* dA \end{aligned} \tag{14}$$

where *(asterisk) indicates complex conjugation of the quantity. Note that when $\mathbf{r}$ $=\mathbf{r}_a$, $\sin(k|\mathbf{r}\text{-}\mathbf{r}_a|)/|\mathbf{r}\text{-}\mathbf{r}_a|$ approaches k and the singularity can be avoided.

Restate Eq. (14) in FE form

$$W = \frac{\rho_0\omega}{4\pi} \sum_i \sum_i v_a^T J_a \frac{\sin k|\mathbf{r} - \mathbf{r}_a|}{|\mathbf{r} - \mathbf{r}_a|} J v^* = \mathbf{V}^*\mathbf{Z}\mathbf{V} \tag{15}$$

Note that single point Gaussian quadrature is used. v_a and v are now the normal velocity at the centroids ($\mathbf{r}_a$ and $\mathbf{r}$) of the element. J_a and J are the values of the Jacobian at the element centers.

The surface velocity can be easily obtained based on results from Eq.(8)

$$\mathbf{V} = -j\omega\mathbf{U}_n \tag{16}$$

$\mathbf{U}_n$ is the normal displacement of the plate, i.e. the transverse displacement component in this paper. Readers can refer to Belegundu et al [1994], Salagame et al [1994], Herrin and Martinus [2003] for more details.

4. Optimization Problem and Sensitivity Analysis

4.1. *Problem formulation*

Besides the acoustic power, the acoustic energy or the weighted sum of the magnitudes of squared pressures are often chosen as the objective functions in structural acoustics. Although slight differences exist, all these physical quantities measure a level of radiated energy [Christensen and Sorokin, 1998].

The topology optimization problem for minimizing the radiated sound power of the bi-material plate in the thermal environment can be stated as

$$\begin{aligned} \min \quad & W = \int_A \frac{1}{2} R_e(pv^*)\mathrm{d}A \\ s.t. \quad & (\mathbf{K} + \mathbf{K}_G - \omega^2\mathbf{M})\mathbf{U} = \mathbf{F} \\ & \mathbf{K}\mathbf{U}_t = \mathbf{F}_t \\ & p = j\rho_0\omega \int_A v_a G(\mathbf{r} - \mathbf{r}_a) dA \\ & \sum_i V_i\zeta_i \le V \\ & \zeta_i \in (0,1) \end{aligned} \tag{17}$$

where ζ_i is the design variable, denoting the artificial volume fraction of material 1 (the stiffer material of the two materials) in the element i; V_i is the volume of the element i; V is the maximum volume of material 1 of the structure.

At each iteration, the second constraint equation is first assembled and solved to calculate the displacement $\mathbf{U}_t$. With Eqs. (5) and (6), the membrane thermal stress σ can be obtained to get the geometric stiffness matrix $\mathbf{K}_\mathrm{G}$. The first constraint equation can then be solved to obtain the structural response. The third constraint equation describes the sound radiation from baffled vibrating plate. Note that the feedback is neglected and it is a sequential vibro-acoustic problem.

4.2. *Sensitivity analysis*

The sensitivity of the objective function W with respect the design variables can be written as

$$\frac{\partial W}{\partial \zeta_i} = \frac{\partial \mathbf{V}^*}{\partial \zeta_i}\mathbf{Z}\mathbf{V} + \mathbf{V}^*\frac{\partial \mathbf{Z}}{\partial \zeta_i} + \mathbf{V} + \mathbf{V}^*\mathbf{Z}\frac{\partial \mathbf{V}}{\partial \zeta_i} = 2\mathbf{V}^*\mathbf{Z}\frac{\partial \mathbf{V}}{\partial \zeta_i} \tag{18}$$

The design variable in this work is the artificial volume fraction of material 1, and the structure is subjected to harmonic load with a prescribed frequency; thus the derivative of matrix $\mathbf{Z}$ to ζ_i is zero. Note that "*the derivative is localized in the sense that the derivative only involves information at the element level*" [Bendsøe and Sigmund, 2003], and the derivative of the velocity $\partial\mathbf{V}/\partial\zeta_i$ in Eq. (18) is in fact $\partial V_i/\partial\zeta_i$. "*However, there is an effect from other design variables hidden* " in the velocity $\mathbf{V}$.

According to Eq. (16), the velocity derivative can be obtained by differentiating Eq. (8)at element level. Note that the harmonic load $\mathbf{F}$ is design-independent.

$$(\mathbf{K}_i + \mathbf{K}_{Gi} - \omega^2\mathbf{M}_i)\frac{\partial\mathbf{U}_i}{\partial\zeta_i} = -\left(\frac{\partial\mathbf{K}_i}{\partial\zeta_i} + \frac{\partial\mathbf{K}_{Gi}}{\partial\zeta_i} - \omega^2\frac{\partial\mathbf{M}_i}{\partial\zeta_i}\right)\mathbf{U}_i \tag{19}$$

Its global form can be written as

$$(\mathbf{K} + \mathbf{K}_{\mathrm{G}} - \omega^2\mathbf{M})\mathbf{U}^{\mathrm{p}} = \mathbf{F}^{\mathrm{p}} \tag{20}$$

where $\mathbf{U}^{\mathrm{p}}$, $\mathbf{F}^{\mathrm{p}}$ can be regarded as pseudo response and load vector. Eq. (20)is a generalized dynamic formula, describing a model that has the same eigenvalues and eigenvectors as Eq. (8)

Using mode superposition, $\mathbf{U}^{\mathrm{p}}$ can be represented as

$$\mathbf{U}^{\mathrm{p}} = \sum_{l}^{m} \lambda_l^p \Phi_l \tag{21}$$

with

$$\lambda_l^p = \sum_{l}^{m} \frac{\mathbf{\Phi}_l^{\mathrm{T}}\mathbf{F}^{\mathrm{P}}}{\omega_{nl}^2 - \omega^2} \tag{22}$$

To obtain $\mathbf{F}^{\mathrm{p}}$, derivatives of the matrices on the right hand of Eq. (19) need to be calculate respectively.

4.2.1. *Derivatives of the stiffness and mass matrices*

It has been shown by Bruyneel et al [2005] and Gao et al [2010] that in SIMP model the volume constraint may not be a binding one and the compliance becomes unbounded in low-density regions for design-dependent problems. The reason is that SIMP has a zero-slope at $\zeta_i = 0$.

RAMP proposed by Stople and Svanberg [2001] turns out to be effective in dealing with such difficulty [Bruyneel et al, 2005; Gao et al, 2010]. The RAMP interpolation models of the elastic modulus, the mass density and the thermal stress

coefficient can be written as

$$E_i = R_E(\zeta_i)E^{(1)} + (1 - R_E(\zeta_i))E^{(0)} \tag{23}$$

$$\rho_i = R_\rho(\zeta_i)\rho^{(1)} + (1 - R_\rho(\zeta_i))\rho^{(0)} \tag{24}$$

$$\beta_i = R_\beta(\zeta_i)\beta^{(1)} + (1 - R_\beta(\zeta_i))\beta^{(0)} \tag{25}$$

where the superscripts 0 and 1 denote material 0 and material 1 respectively;

$$R(\zeta_i) = \frac{\zeta_i}{1 + p(1 - \zeta_i)} \tag{26}$$

and p is the penalty factor. The penalty factors for each material property parameter can be different and p_E, p_ρ, p_β refer to the penalty factors for the elastic modulus, the mass density and the thermal stress coefficient respectively.

The derivatives of $\mathbf{K}$ and $\mathbf{M}$ in Eq. (19) at the element level are as follows

$$\frac{\partial \mathbf{K}_i}{\partial \zeta_i} = \frac{1 + p_E}{(1 + p_E(1 - \zeta_i))^2}(\mathbf{K}_i^{(1)} - \mathbf{K}_i^{(0)}) \tag{27}$$

$$\frac{\partial \mathbf{M}_i}{\partial \zeta_i} = \frac{1 + p_\rho}{(1 + p_\rho(1 - \zeta_i))^2}(\mathbf{M}_i^{(1)} - \mathbf{M}_i^{(0)}) \tag{28}$$

4.2.2. *Derivatives of the geometric stiffness matrix*

The key is the derivative of the geometric stiffness matrix $\mathbf{K}_G$; it involves not only the temperature change, but also the strain induced by the design-dependent equivalent thermal force. With Eq. (4), the membrane stress $\mathbf{S}$ in Eq. (3) can be stated as

$$\mathbf{S} = E\Xi - \beta\Theta \tag{29}$$

where $E\Xi, \beta\Theta$ refer to the strain part and the thermal expansion part respectively. Thus the geometric stiffness matrix can be divided as follows

$$\begin{aligned} \mathbf{K}_{\mathrm{Gi}} &= \sum_i \int_{A_i} \mathbf{G}^{\mathrm{T}} \mathbf{S}_j \mathbf{G} dA \\ &= \sum_i \int_{A_i} \mathbf{G}^{\mathrm{T}} (E_i \Xi_i - \beta_i \Theta_i) \mathbf{G} dA \\ &= \sum_i \int_{A_i} E_i \mathbf{G}^{\mathrm{T}} \Xi_i \mathbf{G} dA - \sum_i \int_{A_i} \beta_i \mathbf{G}^{\mathrm{T}} \Theta_i \mathbf{G} dA \\ &\mathbf{K}_{\mathrm{G}i}^{\mathrm{I}} + \mathbf{K}_{\mathrm{G}i}^{\mathrm{II}} \end{aligned} \tag{30}$$

Accordingly the partial derivative of the geometric stiffness matrix for the element i can be written as

$$\begin{aligned} \frac{\partial \mathbf{K}_{\mathrm{G}i}}{\partial \zeta_i} &= \frac{\partial \mathbf{K}_{\mathrm{G}i}^{I}}{\partial \zeta_i} + \frac{\partial \mathbf{K}_{\mathrm{G}i}^{II}}{\partial \zeta_i} \\ &= \frac{\partial E_i}{\partial \zeta_i} \int_{A_i} \mathbf{G}^{\mathrm{T}} \Xi_i \mathbf{G} dA + E_i \int_{A_i} \mathbf{G}^{\mathrm{T}} \frac{\partial \Xi_i}{\partial \zeta_i} \mathbf{G} dA - \frac{\partial \beta_i}{\partial \zeta_i} \int_{A_i} \mathbf{G}^{\mathrm{T}} \Theta_i \mathbf{G} dA \end{aligned} \tag{31}$$

It can be found that only the second part of the right-hand items is left to deal with, that is, the derivative of the ith element's thermal strain with respect to its artificial volume fraction.

Since the membrane stress $\mathbf{S}$ has been restated as Eq. (29) according to Eq. (4), the derivative of Ξ is in fact equivalent to the derivative of ε, both referring to the derivatives of the membrane strains. It is as follows with Eq. (5)

$$\frac{\partial \varepsilon}{\partial \zeta_i} = \frac{\partial(\mathbf{B}\mathbf{u}_{ti})}{\partial \zeta_i} = \mathbf{B}\frac{\partial \mathbf{u}_{ti}}{\partial \zeta_i} \tag{32}$$

The derivative of the thermal displacement in Eq. (32) can be obtained through differentiate Eq. (6) at the element level

$$\frac{\partial(\mathbf{K}_i\mathbf{U}_{ti})}{\partial \zeta_i} = \frac{\partial \mathbf{F}_{ti}}{\partial \zeta_i} \tag{33}$$

$$\mathbf{K}_i\frac{\partial \mathbf{U}_{ti}}{\partial \zeta_i} = -\frac{\partial \mathbf{K}_i}{\partial \zeta_i}\mathbf{U}_{ti} + \frac{\partial \mathbf{F}_{ti}}{\partial \zeta_i} \tag{34}$$

Note that $\mathbf{F}_t$ is design-dependent and related to the thermal stress coefficient β; its derivative is non-zero. According Eq. (7), the derivation of $\mathbf{F}_t$can be written as

$$\frac{\partial \mathbf{F}_{ti}}{\partial \zeta_i} = \frac{\partial \beta_i}{\partial \zeta_i}\int_{A_i} \mathbf{B}^{\mathrm{T}}\mathbf{D}\mathbf{\Gamma} dA \tag{35}$$

The global form of Eq. (34) should be assembled and then solved with the boundary conditions to obtain the derivative of thermal displacement in Eq. (32).

So far, the derivative of the geometric stiffness matrix $\mathbf{K}_G$ has been obtained, and the sensitivity analysis is now finished.

5. Numerical Example

A four-edge clamped bi-material square plate with dimension 1m×1m×0.02m is studied. The plate is subjected to a temperature rise $\Delta T = T_1 - T_0$with $T_0 = 0°$. The specific mass of the fluid (i.e. air) is $\rho_0 = 1.21$ and the sound speed $c = 343.4$m/s. The material properties are as follows:
$E^{(0)} = 70$GPa, $\rho^{(0)} = 2650$kg/m^3, $\alpha^{(0)} = 1.5 \times 10^{-5\circ-1}$
$E^{(1)} = 210$GPa, $\rho^{(1)} = 6500$kg/m^3, $\alpha^{(1)} = 1.1 \times 10^{-5\circ-1}$
A mesh of 40×40 with isoparametric 4-node element is used here. The control volume fraction of material 1 is 50%, uniformly distributed for the initial structure. A harmonic concentrated load with 1N amplitude is applied at the quarter-point (0.25, 0.25) of the plate. $p_E = p_\rho = 3$ and $p_\beta = 0$ used in the following calculations.

Both Eqs. (19) and (34) need to be solved during the sensitivity analysis, and the property of the sensitivity is intricate, and the dynamic compliance may possibly be non-monotonous. GCMMA [Svanberg, 1995], the globally convergent version of MMA [Svanberg, 1987] is employed.

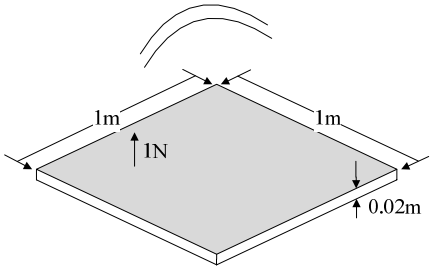

Fig. 1. Acoustic radiation from the four-edge clamped square plate driven by an unit harmonic concentrated load.

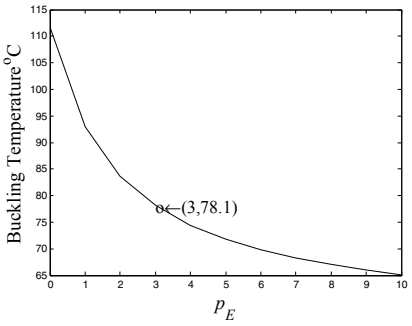

Fig. 2. The critical buckling temperature of the initial plate.

5.1. *Eigenvalue and buckling analysis*

T_{cr} is first evaluated by carrying out an eigenvalue buckling analysis Eq. (1). It serves as the upper limit of ΔT, to ensure that the uniform temperature rise does not induce buckling of the initial plate.

According to Fig. 2, four thermal cases, i.e. $\Delta T = 0°, \Delta T = 40°$, $\Delta T = 60°, \Delta T = 70°$, are chosen for analysis in this work. It is shown later from the numerical results that T_{cr} increases as the optimization proceeds, indicating that the plate is always in the pre-buckling state.

The first two natural frequencies and mode shapes of the initial plate in the four thermal conditions are shown in Table 1 and Fig. 3 respectively. Although the natural frequencies decrease obviously, the mode shapes hardly change. According to the eigen-analysis, two excitation-frequency cases, $f = 50$Hz and $f = 250$Hz, are chosen and studied.

Table 1. First two natural frequencies

	$\Delta T = 0°$	$\Delta T = 40°$	$\Delta T = 60°$	$\Delta T = 70°$
1^{st}	184.1Hz	129.7 Hz	89.9 Hz	60.4 Hz
2^{nd}	375.1 Hz	317.0 Hz	283.1 Hz	264.4 Hz

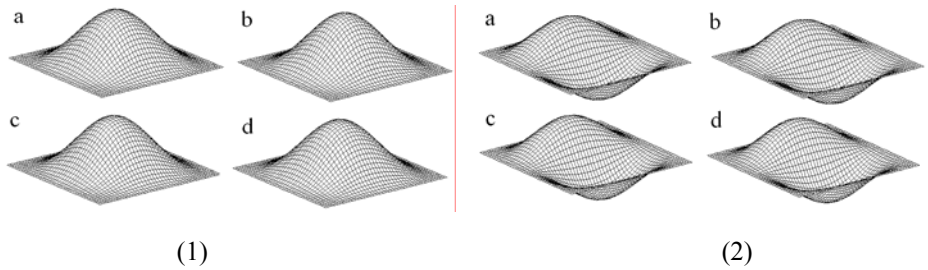

Fig. 3. (1) 1st and (2) 2nd mode shapes in the four thermal environments a $\Delta T = 0°$, b $\Delta T = 40°$, c $\Delta T = 60°$, d $\Delta T = 70°$.

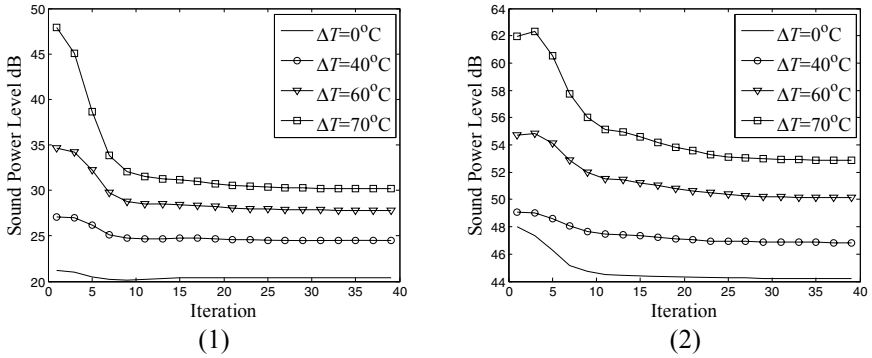

Fig. 4. Iteration history of the sound power level of (1) case $f = 50$Hz and (2) case $f = 250$Hz.

5.2. *Results and discussions*

The iteration history of the sound power level (SPL) is shown in Fig. 4.

For case $f = 50$Hz, the SPL is 21.2dB, 27.1dB, 34.6dB, 47.9 dB initially and decreases 3%, 10.6%, 19.8% and 36.7% respectively after optimization. As the temperature rises, the natural frequencies decrease and the structure tends to resonate; thus the SPL becomes higher.

For case $f = 250$Hz, the increase of SPL with temperature implies that the second natural frequency is probably the main component that affects the response. If this is not the case, then the fundamental frequency one will be the main component. Due to the fact that the natural frequencies decrease with the temperature, SPL verse the temperature could not be monotonous.

The optimal topology in the four thermal cases is shown in Fig. 5. Rayleigh integral indicates that the SPL is only related to the normal velocity; thus, so will be the distribution of the stiffer material (material 1) in the optimization. The change of the topology also reflects the effect of the thermal environment on the normal velocity.

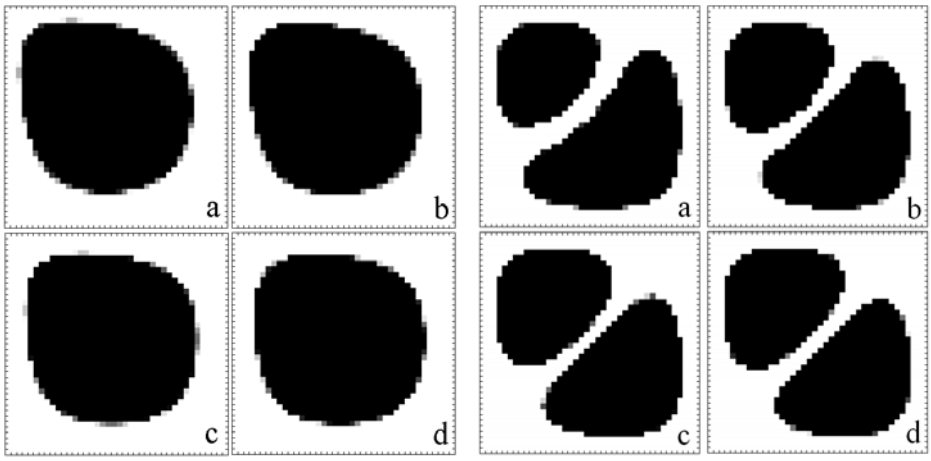

Fig. 5. Topology of the bi-material plate (white: material 0; black: material 1) with (1)$f = 50$Hz and (2) $f = 250$Hz in the four thermal environments a $\Delta T = 0°$, b $\Delta T = 40°$, c $\Delta T = 60°$, d $\Delta T = 70°$.

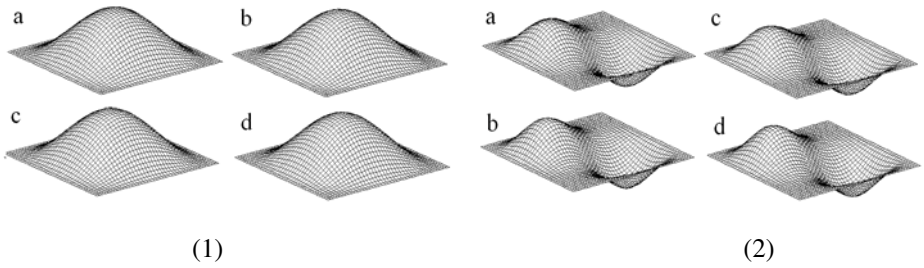

Fig. 6. (1)1$^{\text{st}}$ mode shape for the case $f = 50$Hz and (2) 2$^{\text{nd}}$ mode shape for the case f=250Hz of the optimal plate after optimization in the four thermal environments a $\Delta T = 0°$, b $\Delta T = 40°$, c $\Delta T = 60°$, d $\Delta T = 70°$.

The first mode shape of the optimal plate after optimization for the case $f = 50$Hz is shown in Fig. 6(1). There is barely change compared to Fig. 3(1). The second mode shape of the optimal plate for the case $f = 250$Hz is shown in Fig. 6(2). It is initially symmetrical with respect to the midline in Fig. 3(2) and now symmetrical (not absolutely symmetrical) with respect to the diagonal.

For the lower-temperature subcases of the case $f = 50$Hz, more material 1 lumps around the location of the applied load. As the structure tends to resonate with the temperature rise, the material moves towards the center and the pattern of the topology becomes more and more similar to that the mode shape. Note that the mode shape suggests the resonance normal velocity (or displacement) at the associated natural frequency.

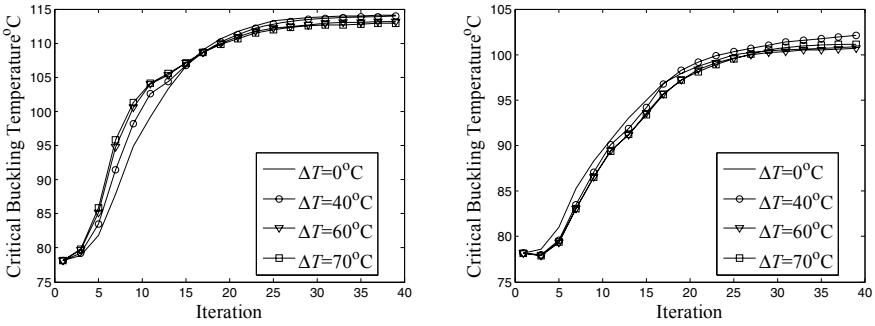

Fig. 7. Tteration history of the critical buckling temperature of (1) case $f = 50$Hz and (2) case $f = 250$Hz.

For the case $f = 250$Hz, as the temperature rises, the upper part becomes larger and its pattern resembles that of the second mode shape more closely, which also indicates that the topology is mainly affected by the second natural frequency other than the first.

During the optimization process, $T_{\rm cr}$ is monitored to check whether the plate is pre-buckling state to ensure that Eq.(8) can be used. It is shown in Fig. 7 that $T_{\rm cr}$ increases as the iteration grows, indicating that no bifurcation occurs. In some sense, it means that the optimization yields a stiffer structure.

6. Conclusion

In this paper structural topology optimization in a thermal environment with respect to the radiated acoustic characteristic is investigated for the first time. The thermal stress is regarded as pre-stress, through which the dynamic formula is obtained to evaluate the structural response. The radiation sound power can then be calculated by Rayleigh integral. Sensitivity analysis is carried out in which the derivative of the geometric stiffness matrix is the key point.

A bi-material plate subjected to a harmonic force with prescribed amplitude and frequency is studied. Through buckling and eigenvalue analysis, four pre-buckling thermal cases and two excitation frequency cases are chosen. Numerical results show that the natural frequencies decrease with the increase of the temperature, the structure approaches to resonance; thus the radiated sound power level becomes higher. The pattern of the optimal topology resembles that of the mode shape more closely, which is due to the fact that only the normal velocity is needed in the Rayleigh integral to calculate the radiated sound power. It also shows that during the optimization process, the critical buckling temperature increases and the structure is always in the pre-buckling state.

Acknowledgment

The assistance on the GCMMA algorithm from Prof. Svanberg K is gratefully acknowledged.

References

Akl, W., El-Sabbagh A. and Al-Mitani, K. et al., [2009] "Topology optimization of a plate coupled with acoustic cavity," *Int J Solids Struct*, **46**, 2060–2074.

Belegundu, A. D., Salagame, R. R. and Koopmann, G. H. [1994] "A general optimization strategy for sound power minimization," *Struct Optim*, **8**, 113–119.

Bendsøe, M. P. and Kikuchi, N. [1988] "Generating optimal topologies in structural design using a homogenization method," *Comput Methods Appl Mech Eng*, **71**, 197–224.

Bendsøe, M. P. and Sigmund, O. [2003] *Topology optimization theory methods and applications* (Springer. Berlin).

Bruyneel, M. and Duysinx, P. [2005] "Note on topology optimization of continuum structures including self-weight," *Struct Multidiscip Optim*, **29**, 245–256.

Christensen, S. T., Sorokin, S. V. and Olhoff, N. [1988] "On analysis and optimization in structural acoustics," *Struct Optim*, **16**, 83–107.

Cook, R. D. [1994] *Finite Element Modeling for Stress Analysis* (John Willy & Sons. New York).

Du, J. and Olhoff, N. [2007] "Minimization of sound radiation from vibrating bi-material structures using topology optimization," *Struct Multidisc Optim*, **33**, 305–321.

Du, J. and Olhoff, N. [2010] "Topological design of vibrating structures with respect to optimum sound pressure characteristics in a surrounding acoustic medium," *Struct Multidisc Optim*, **42**, 43–54.

Gao, T. and Zhang, W. [2010] "Topology optimization involving thermo-elastic stress loads," *Struct Multidisc Optim*, **42**, 725–738.

Herrin, D. W., Martinus, F. and Wu, T. W. et al., [2003]. "A New Look at the High Frequency Boundary Element and Rayleigh Integral Approximations," *SAE Noise & Vibration Conference and Exhibition*, May 2003, Grand Traverse, MI, USA.

Kim, N. H., Dong, J., Choi, K. K. et al., [2003] "Design sensitivity analysis for a sequential structural–acoustic problem," *J Sound Vib*, **263**, 569–591.

Kim, N. H. and Dong, J. [2006] "Shape sensitivity analysis of sequential structural–acoustic problems using FEM and BEM". *J Sound Vib*, **290**, 192–208.

Lee, J. and Wang, S. Y. [2003] "Shape Design Sensitivity Analysis for the Radiated Noise from the Thin-Body". *J Sound Vib*, **261**, 895–910.

Lee, J., Wang, S. Y. and Dikec, A. [2004] "Topology optimization for the radiation and scattering of sound from thin-body using genetic algorithms," *J Sound Vib*, **276**, 899–918.

Luo, J. H. and Gea, H. G. [2003] "Optimal Stiffener Design for Interior Sound Reduction Using a Topology Optimization Based Approach," *J Sound Vib*, **125**, 267–273.

Ma, Z. D. and Hagiwara, I. [1991] "Sensitivity Analysis Methods for Coupled Acoustic-Structural Systems," *AIAA J*, **29**, 1787–1801.

Pedersen, N. L. [2001] "On topology optimization of plates with prestress," *Int J Numer Meth Engng*, **51**, 225–239.

Pedersen, N. L. [2002] "Topology optimization of laminated plates with prestress," *Computers Structures*, **80**, 559–570.

Rodrigues, H. and Fernandes, P. [1995] "A material based model for topology optimization of thermoelastic structures," *Int J Numer Methods Engng*, **38**, 1951–1965.

Rozvany, GIN [2001] "On design-dependent constraints and singular topologies," *Struct Multidisc Optim*, **21**, 164–172.

Salagame, R. R., Belegundu, A. D. and Koopmann, G. H. [1994] "Analytical sensitivity of acoustic power radiated from plates," *J Vib Acoust*, **117**, 43–48.

Stolpe, M. and Svanberg, K. [2001] "An alternative interpolation scheme for minimum compliance topology optimization," *Struct Multidisc Optim*, **22**, 116–124.

Svanberg, K. [1987] "The method of moving asymptotes—a new method for structural optimization," *Int J Numer Methods Engng*, **24**, 359–373.

Svanberg, K. [1995] "A globally convergent version of MMA without linesearch," *First world congress of structural and multidisciplinary optimization*. Pergamon, Oxford, 9–16.

Yoon, G. H., Jensen, J. S. and Sigmund, O. [2007] "Topology optimization of acoustic-structure interaction problems using a mixed finite element formulation," *Int J Numer Methods Engng*, **70**, 1049–1075.

Zienkiewicz, O. C. and Taylor, R. L. [2005] *The Finite Element Method for Solid and Structural Mechanics (Sixth edn)*, (Butterworth–Heinemann: Elsevier, London).